Optimal Design of Heterogeneous Materials

S. Torquato

Department of Chemistry, Department of Physics, Princeton Center for Theoretical Science, and Princeton Institute for the Science and Technology of Materials, Princeton University, Princeton, New Jersey 08544; email: torquato@electron.princeton.edu

Annu. Rev. Mater. Res. 2010. 40:101–29

First published online as a Review in Advance on March 25, 2010

The *Annual Review of Materials Research* is online at matsci.annualreviews.org

This article's doi: 10.1146/annurev-matsci-070909-104517

1531-7331/10/0804-0101$20.00

Key Words

microstructure, optimization, statistical correlation functions, topology, reconstruction

Abstract

This article reviews recent inverse techniques that we have devised to optimize the structure and macroscopic properties of heterogeneous materials such as composite materials, porous media, colloidal dispersions, and polymer blends. Optimization methods provide a systematic means of designing materials with tailored properties and microstructures for a specific application. This article focuses on two inverse problems that are solved via optimization techniques: (*a*) the topology optimization procedure used to design heterogeneous materials and (*b*) stochastic optimization methods employed to reconstruct or construct microstructures.

1. INTRODUCTION

A holy grail of materials science is to have exquisite knowledge of structure/property relations to design material microstructures with desired properties and performance characteristics. Although this objective has been achieved in certain cases through trial and error, a systematic means of doing so is currently lacking. For certain physical phenomena at specific length scales, the governing equations are known, and the only barrier to achieving the aforementioned goal is the development of appropriate methods to attack the problem. Often, this objective can be achieved for heterogeneous materials.

A heterogeneous material is composed of domains of different materials (phases), such as a composite, or the same material in different states, such as a polycrystal (1). It is assumed that the "microscopic" length scale is much larger than the molecular dimensions but much smaller than the characteristic length of the macroscopic sample. In such circumstances, the heterogeneous material can be viewed as a continuum on the microscopic scale, and macroscopic or effective properties can be ascribed to it (see **Figure 1**). Heterogeneous materials abound in synthetic products and nature. Synthetic examples include aligned and chopped fiber composites, particulate composites, powders, interpenetrating multiphase composites, cellular solids, colloids, gels, foams, phase-separated metallic alloys, microemulsions, block copolymers, and fluidized beds. Some examples of natural heterogeneous materials are granular media, soils, polycrystals, sandstone, wood, bone, lungs, blood, animal and plant tissue, cell aggregates, and tumors. The physical phenomena of interest occur on microscopic length scales that span from tens of nanometers in the case of gels to meters in the case of geological media. Structure on this microscopic scale is generically referred to as microstructure.

The theoretical prediction of the transport, electromagnetic, and mechanical properties of heterogeneous materials has a long and venerable history, attracting the attention of some of the luminaries of science, including Maxwell (2), Lord Rayleigh (3), and Einstein (4). Since the early work on the physical properties of heterogeneous materials, there has been an explosion in the literature on this subject (1, 5–10) because of the rich and challenging fundamental problems it offers and its manifest technological importance.

Consider a two-phase heterogeneous material consisting of a phase with a property K_1 and volume fraction ϕ_1 and another phase with a property K_2 and volume fraction ϕ_2 $(=1-\phi_1)$.

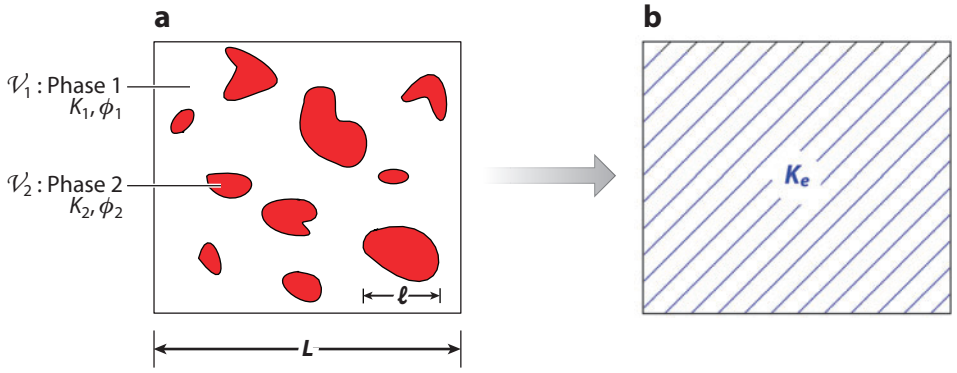

Figure 1

(*a*) A schematic of a random two-phase material [shown as *white* ($\mathcal{V}_1$) and *red* ($\mathcal{V}_2$) *regions*] with general phase properties K_1 and K_2 and phase volume fractions ϕ_1 and ϕ_2, as adapted from Torquato (1). Here L and ℓ represent the macroscopic and microscopic length scales, respectively. (*b*) When L is much bigger than ℓ, the heterogeneous material can be treated as a homogeneous material with effective property $\mathbf{K}_e$.

(The extension to M phases, where $M \geq 2$, is straightforward.) The property K_i is perfectly general: It may represent a transport, mechanical, or electromagnetic property or properties associated with coupled phenomena, such as piezoelectricity or thermoelectricity, or with wave propagation characteristics (e.g., band gaps). Depending upon the physical phenomenon of interest, one must solve for the relevant local fields (e.g., electric field, concentration field, or stress field), which are solutions to partial differential equations (e.g., steady-state heat or electrical conduction, Maxwell's electrodynamic equations, or Stokes equations for slow viscous flow) subject to boundary and initial conditions.

Effective properties of interest include, but are not limited to, the following examples:

1. effective thermal (electrical) conductivity,
2. effective diffusion coefficient,
3. effective dielectric constant,
4. effective elastic moduli,
5. mean survival time of a Brownian particle,
6. fluid permeability,
7. effective thermal expansion coefficients,
8. effective piezoelectric coefficients, and
9. effective wave characteristics.

One can show that the effective tensor property $\mathbf{K}_e$ often (but not always) is found by homogenizing (averaging) the aforementioned local fields (1, 9). In the case of linear material, for example, the effective property $\mathbf{K}_e$ is given by

$$\langle \mathbf{F}(\mathbf{r}) \rangle = \mathbf{K}_e \cdot \langle \mathbf{G}(\mathbf{r}) \rangle, \qquad 1.$$

where $\mathbf{F}$ represents some generalized flux (e.g., current or stress), $\mathbf{G}$ represents some generalized gradient (e.g., electric field or strain), and angular brackets denote a volume average and/or an ensemble average.

A systematic theory of random heterogeneous materials rests on our ability to describe the details of the microstructure, by which we mean the phase volume fractions; surface areas of interfaces, orientations, sizes, shapes, and spatial distribution of the phase domains; connectivity of the phases; etc. Quantitatively speaking, we can statistically characterize the microstructure by certain n-point correlation functions (1), some of which are defined in Section 3 below. The general effective property $\mathbf{K}_e$ is the following function:

$$\mathbf{K}_e = f(K_1, K_2; \phi_1, \phi_2; \boldsymbol{\Omega}), \qquad 2.$$

where $\boldsymbol{\Omega}$ indicates functionals of higher-order microstructural information, i.e., integrals of the local fields weighted with the relevant statistical correlation functions (1). The mathematical form that this microstructural information takes depends on the underlying local fields for the particular physical phenomenon being studied.

Thus, we see from Equation 2 that, given the phase properties and microstructure, one can in principle predict the effusive property of interest. This is the forward problem, which is the natural and standard approach taken in the theory of heterogeneous materials. The forward problem has been solved using theoretical techniques (1, 9–21) and computational methods (22–32).

However, equally important questions can be posed as inverse problems, i.e., how does one spatially distribute the phases of a heterogeneous material to optimize or target some macroscopic behavior or statistical properties of the heterogeneous material? Inverse problems are well suited to be solved via optimization techniques. Optimization methods provide a systematic means of designing heterogeneous materials with tailored properties and microstructures for a specific application. This article reviews progress that we have made on the implementation and application

of two inverse problems that are solved using optimization techniques: (*a*) the topology optimization procedure used to design heterogeneous materials and (*b*) stochastic optimization methods employed to reconstruct or construct such microstructures given limited but targeted structural information.

2. TOPOLOGY OPTIMIZATION

A promising method for the systematic design of composite microstructures with desirable macroscopic properties is the topology optimization method. The topology optimization method was developed more than two decades ago by Bendsøe & Kikuchi (33) for the design of mechanical structures. Currently, it is also being used in smart and passive material design, mechanism design, microelectromechanical systems (MEMS) design, target optimization, multifunctional optimization, and other design problems (34–40).

2.1. Problem Statement

The basic topology optimization problem can be stated as follows: the distribution of a given amount of material in a design domain such that an objective function is extremized (33, 34, 36, 40). The design domain is the periodic base cell and is initialized by discretizing it into a large number of finite elements (see **Figure 2**) under periodic boundary conditions. The problem consists in finding the optimal distribution of the phases (solid, fluid, or void) such that the objective function is minimized. The objective function can be any combination of the individual components of the relevant effective property tensor subject to certain constraints (34, 40). For

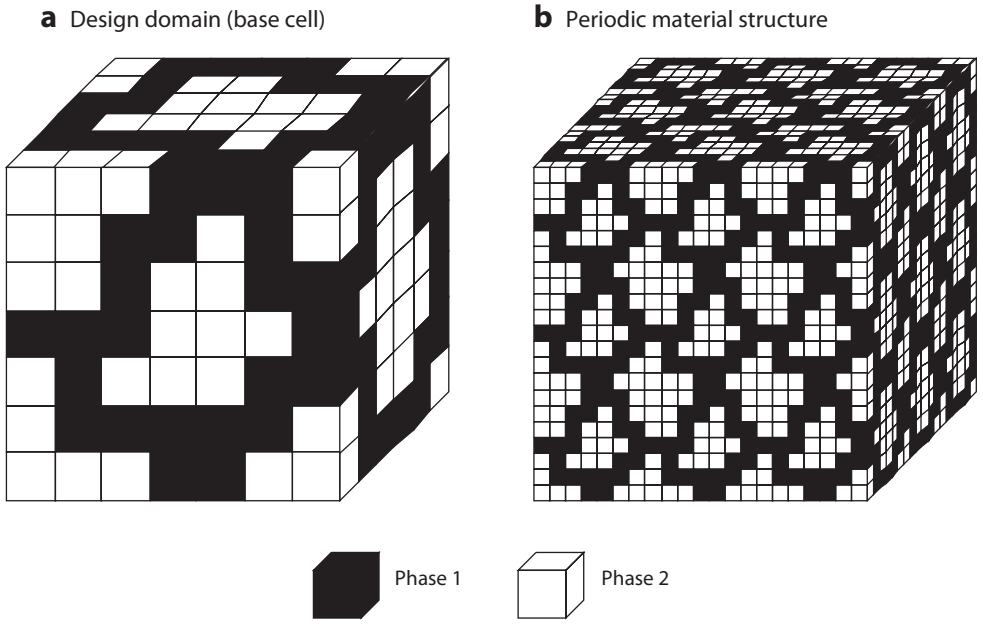

Figure 2

Design domain and discretization for a two-phase, three-dimensional topology optimization problem. Each cube represents one finite element, which can consist of either phase 1 material or phase 2 material.

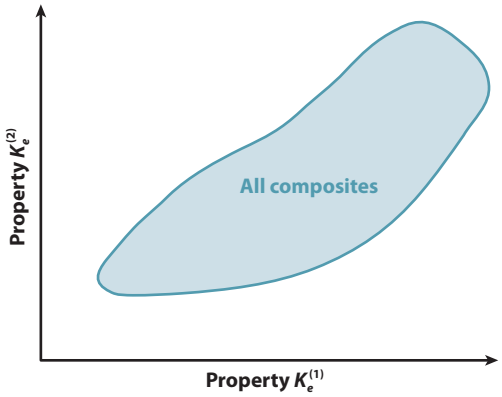

Figure 3

Schematic illustrating the allowable region in which all composites with specified phase properties must lie for the case of two different effective properties, as adapted from Torquato et al. (39).

target optimization (37) and multifunctional optimal design (38, 39), the objective function can be appropriately modified, as described below. In the most general situation, it is desired to design a composite material with M different effective properties, which we denote by $K_e^{(1)}, K_e^{(2)}, \ldots, K_e^{(M)}$, given the individual properties of the phases.

In principle, one wants to know the region (set) in the multidimensional space of effective properties in which all composites must lie (see **Figure 3**). The size and shape of this region depend on how much information about the microstructure is specified and on the prescribed phase properties. For example, the set in which even the volume fractions are not specified is clearly larger than the one in which the volume fractions are specified. The determination of the allowable region is generally a highly complex problem. However, the identification of the allowable region can be greatly facilitated if cross-property bounds on the effective properties are found. Cross-property bounds are inequalities that rigorously link different effective properties to one another. For example, links between different transport properties (1, 9, 41–47) and between the conductivity and elastic moduli (47–51) have been established. When cross-property bounds are optimal (i.e., the best possible bounds), they can be used to identify the boundary of the allowable region. Numerical optimization methods (34, 36, 38–40, 52–54) can subsequently be employed to discover the specific composite microstructures that lie on the boundary.

To solve the numerical optimization problem, one could begin by making an initial guess for the distribution of the two phases among the elements (see **Figure 2**), solving for the local fields using finite elements, and then evolving the microstructure to the targeted properties. However, even for a small number of elements, this integer-type optimization problem becomes a huge and intractable combinatorial problem. For example, for a small design problem with $N = 100$, the number of different distributions of the three material phases would be astronomically large ($3^{100} = 5 \times 10^{47}$). Because each function evaluation requires a full finite element analysis, it is hopeless to solve the optimization problem using random search methods such as genetic algorithms or simulated annealing methods, which use a large number of function evaluations and do not make use of sensitivity information.

Following the idea of standard topology optimization procedures, the problem is therefore relaxed by allowing the material at a given point to be a gray-scale mixture of the two phases, which defines a local density. This makes it possible to linearize the objective function about the current local density and find sensitivities (i.e., gradients) with respect to design changes

(i.e., changes in local density). One can then exploit well-established and powerful linear programming methods (55) to solve the optimization problem. The optimization procedure solves a sequence of finite element problems followed by changes in material type (density) of each of the finite elements, based on sensitivities of the objective function and constraints with respect to design changes. At the end of the optimization procedure, however, we desire to have a design in which each element is either a phase 1 material or a phase 2 material. This is achieved by imposing a penalization for gray phases at the final stages of the simulation.

In the relaxed system, we let $x_i \in [0, 1]$ be the local density of the ith element, so that when $x_i = 0$, the element corresponds to phase 1 and when $x_i = 1$, the element corresponds to phase 2. Let $\mathbf{x}$ $(x_i, i = 1, \ldots, n)$ be the vector of design variables that satisfies the constraint for the fixed volume fraction $\phi_2 = \langle x_i \rangle$. For any $\mathbf{x}$, the local fields are computed using the finite element method, and the effective property $K_e(K; \mathbf{x})$, which is a function of the material property K and $\mathbf{x}$, is obtained by the homogenization of the local fields. The optimization problem is specified as follows:

$$\begin{aligned} &\text{Minimize} : \Phi = K_e(x) \\ &\text{subject to} : \frac{1}{n}\sum_{i=1}^{n} x_i = \phi_2 \\ &0 \le x_i \le 1, \quad i = 1, \ldots, n \\ &\text{and prescribed symmetries.} \end{aligned} \qquad 3.$$

The objective function $K_e(\mathbf{x})$ is generally nonlinear. To solve this problem, we linearize it, enabling us to take advantage of powerful sequential linear programming techniques. Specifically, the objective function is expanded in Taylor series for a given microstructure $\mathbf{x}_0$:

$$\Phi \simeq K_e(\mathbf{x}_0) + \nabla K_e \cdot \Delta\mathbf{x}, \qquad 4.$$

where $\Delta\mathbf{x} = \mathbf{x} - \mathbf{x}_0$ is the vector of density changes. In each iteration, the microstructure evolves to the optimal state by determining the small change $\Delta\mathbf{x}$. One can use the simplex method (34) or the interior-point method (37) to minimize the linearized objective function in Equation 4. In each iteration, the homogenization step to obtain the effective property $K_e(K; \mathbf{x}_0)$ is carried out numerically via the finite element method on the given configuration $\mathbf{x}_0$. Derivatives of the objective function (∇K_e) are calculated by a sensitivity analysis, which requires one finite element calculation for each iteration.

One can use the topology optimization to design at will composite microstructures with targeted effective properties under required constraints (37). The objective function Φ for such a target optimization problem is chosen to be given by a least-square form involving the effective property $K_e(\mathbf{x})$ at any point in the simulation and a target effective property K_0:

$$\Phi = [K_e(\mathbf{x}) - K_0]^2. \qquad 5.$$

The method can also be employed for multifunctional optimization problems. The objective function Φ in this instance is chosen to be a weighted average of each of the effective properties (38).

2.2. Illustrative Examples

The topology optimization procedure has been employed to design composite materials with extremal properties (34, 35, 56), targeted properties (37, 52), and multifunctional properties (38, 39). To illustrate the power of the method, we briefly describe microstructure designs in which thermal expansion and piezoelectric behaviors are optimized, the effective conductivity achieves

a targeted value, and the thermal conduction demands compete with the electrical conduction demands. The latter design turns out to be optimal when the bulk modulus competes with conduction or diffusion properties, and appears to have other optimized transport properties. We close with some remarks about optimizing band gaps associated with wave propagation.

2.2.1. Unusual thermal expansion behavior. Materials with extreme or unusual thermal expansion behavior are of interest from both a technological and a fundamental standpoint. Zero-thermal-expansion materials are needed in structures subject to temperature changes, such as space structures, bridges, and piping systems. A negative-thermal-expansion material has the counterintuitive property of contracting upon heating. A fastener made of a negative-thermal-expansion material, upon heating, can be inserted easily into a hole. Upon cooling, it will expand, fitting tightly into the hole. Materials with large thermal displacement or force can be employed as thermal actuators.

All three of these types of expansion behavior have been optimally designed (34), but here we briefly describe the first two cases. In the negative-expansion case, one must consider a three-phase material: a high-expansion material, a low-expansion material, and a void region. **Figure 4*a*** shows the two-dimensional optimal design (design I) that was found. The red phase has a thermal expansion coefficient that is 10 times larger than that of the blue phase. The main mechanism behind the negative-expansion behavior is the reentrant cell structure having bimaterial components that bend (into the void space) and cause large deformations when the temperature increases. Design II in **Figure 4*b*** shows an example in which the effective bulk modulus is maximized subject to the constraint that the effective thermal coefficient be exactly zero. Both designs have effective thermal expansion coefficients that lie very close to rigorous bounds on the effective thermal expansion coefficient for three-phase materials derived by Gibiansky & Torquato (57), indicating that these designs are essentially globally optimal solutions.

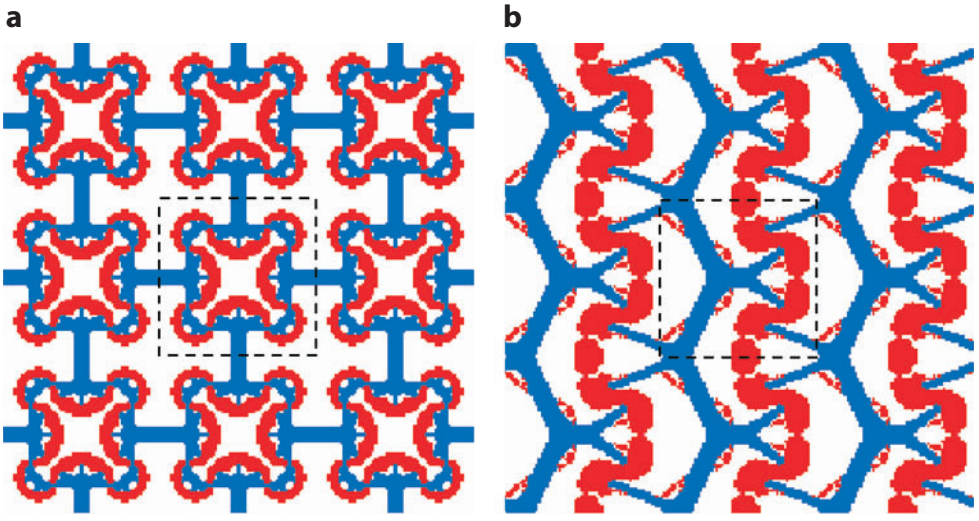

Figure 4

(*a*) Design I: optimal microstructure for minimization of the effective thermal expansion coefficient (34). White regions denote void, blue regions consist of low-expansion material, and red regions consist of high-expansion material. (*b*) Design II: optimal microstructure in which the effective bulk modulus is maximized subject to the constraint that thermal expansion be exactly zero (34).

2.2.2. Piezoelectrics. In the case of piezoelectricity, actuators that maximize the delivered force or displacement can be designed. Moreover, one can design piezocomposites (consisting of an array of parallel piezoceramic rods embedded in a polymer matrix) that maximize the sensitivity to acoustic fields. The topology optimization method has been used to design piezocomposites with optimal performance characteristics for hydrophone applications (35). When one is designing for maximum hydrostatic charge coefficient, the optimal transverse isotropic matrix material has negative Poisson's ratio in certain directions. This matrix material turns out to be a composite, namely, a special porous solid. Using an AutoCAD file of the three-dimensional matrix material structure and a stereolithography technique, researchers have fabricated such negative-Poisson's-ratio materials (35). Corresponding theoretical studies have supported these numerical results (58–60).

2.2.3. Target optimization. Let us now consider the use of topology optimization techniques to design materials with targeted properties. For the case of a two-phase, two-dimensional, isotropic composite, the popular effective-medium approximation (EMA) formula for the effective electrical conductivity σ_e is given by

$$\phi_1 \left[\frac{\sigma_e - \sigma_1}{\sigma_e + \sigma_1} \right] + \phi_2 \left[\frac{\sigma_e - \sigma_2}{\sigma_e + \sigma_2} \right] = 0, \qquad 6.$$

where ϕ_i and σ_i are the volume fraction and the conductivity of phase i, respectively. Milton (61) showed that the EMA expression is exactly realized by granular aggregates of the two phases such that spherical grains (in any dimension) of comparable size are well separated with self-similarity on all length scales. This is why the EMA formula breaks down when applied to dispersions of identical circular inclusions. An interesting question is the following: Can the EMA formula be realized by simple structures with a single length scale? Using the target optimization formulation in which the target effective conductivity σ_0 is given by the EMA function (6), Torquato & Hyun (52) found a class of periodic, single-scale dispersions that achieve it at a given phase conductivity ratio for a two-phase, two-dimensional composite over all volume fractions. Moreover, to an excellent approximation (but not exactly), the same structures realize the EMA for almost the entire range of phase conductivities and volume fractions. The inclusion shapes are given analytically by the generalized hypocycloid, which in general has a nonsmooth interface (see **Figure 5**).

2.2.4. Multifunctional optimization and minimal surfaces. A variety of performance demands are increasingly being placed on material systems. Multifunctional requirements include component structures that have desirable mechanical, thermal, electromagnetic, chemical, and flow properties and low weight. It is difficult to find single homogeneous materials that possess these multifunctional characteristics. Composite materials are ideally suited to achieve multifunctionality because the best features of different materials can be combined to form a new material that has a broad spectrum of desired properties. The ultimate multifunctional materials are provided by nature; virtually all biological material systems are composites that typically are endowed with a unique set of properties.

Minimal surfaces necessarily have zero mean curvature, i.e., the sum of the principal curvatures at each point on the surface is zero. Particularly fascinating are minimal surfaces that are triply periodic because they arise in a variety of systems, including block copolymers, nanocomposites, micellar materials, and lipid-water systems (38). These two-phase composites are bicontinuous in the sense that the surface (two-phase interface) divides space into two disjoint but intertwining phases that are simultaneously continuous. This topological feature of bicontinuity is rare in two dimensions and is therefore virtually unique to three dimensions (1).

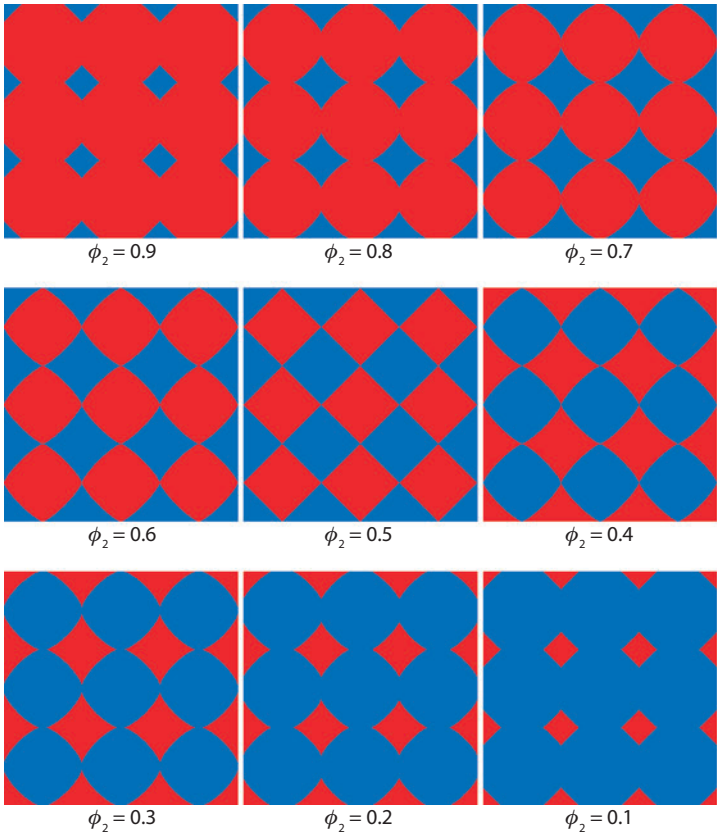

Figure 5

Unit cells of generalized hypocycloidal inclusions in a matrix that realize the effective-medium approximation (EMA) relation (1) for selected values of the volume fraction in the range $0 < \phi_2 < 1$. Phases 1 and 2 are the blue and the red phases, respectively (59).

Using multifunctional optimization (38), investigators have discovered that triply periodic, two-phase, bicontinuous composites with interfaces that are the Schwartz P and D minimal surfaces (see **Figure 6**) are not only geometrically extremal but extremal for simultaneous transport of heat and electricity. More specifically, these are the optimal structures when a weighted sum of the effective thermal and electrical conductivities ($\Phi = \lambda_e + \sigma_e$) is maximized for the case in which phase 1 is a good thermal conductor but a poor electrical conductor and phase 2 is a poor thermal conductor but a good electrical conductor with $\phi_1 = \phi_2 = 1/2$. The demand that this sum be maximized sets up a competition between the two effective transport properties, and this demand is met by the Schwartz P and D structures. By mathematical analogy, the optimality of these bicontinuous composites applies to any of the pairs of the following scalar effective properties: electrical conductivity, thermal conductivity, dielectric constant, magnetic permeability, and diffusion coefficient. It will be of interest to investigate whether the optimal structures when $\phi_1 \neq \phi_2$ are bicontinuous structures with interfaces of constant mean curvature, which would become minimal surfaces at the point $\phi_1 = \phi_2 = 1/2$.

The topological property of bicontinuity of these structures suggests that they would be mechanically stiff even if one of the phases were a compliant solid or a liquid, provided that the other

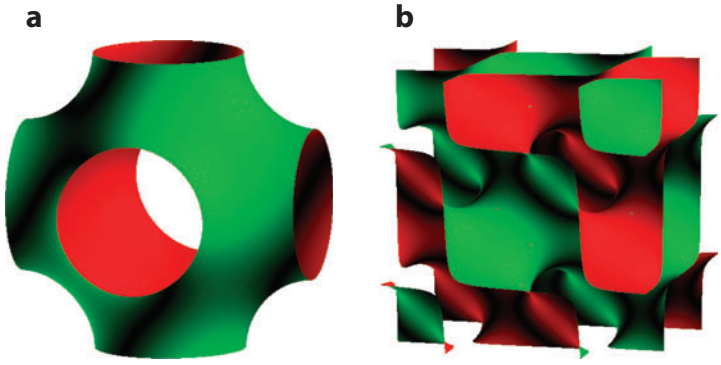

Figure 6

Unit cells of two different minimal surfaces with a resolution of 64 × 64 × 64, as taken from Torquato et al. (38). (*a*) Schwartz D surface. (*b*) Schwartz P surface.

phase were a relatively stiff material. Indeed, it has recently been shown that the Schwartz P and D structures are extremal when a competition is set up between the bulk modulus and the electrical (or thermal) conductivity of the composite (62).

The Schwartz P porous medium has the largest fluid permeability among members of a relatively large class of triply periodic porous media (63). Similarly, a porous medium with a perfectly absorbing interface that is the Schwartz P minimal surface maximizes the mean survival time of a Brownian particle among the members of the aforementioned class of triply periodic porous media (64). This adds to the growing evidence of the multifunctional optimality of this bicontinuous porous medium. Two of the most well-known triply periodic minimal surfaces are the Schwartz P and Schwartz D surfaces. Whereas the former has cubic symmetry, the latter has diamond symmetry; see Reference 38 and references therein for additional details.

The fluid permeabilities and mean survival times for this class of triply periodic porous media are inversely proportional to their corresponding specific surfaces (i.e., interface surface areas per unit volume) (63, 64). This has led to the conjecture that the maximal fluid permeability and the maximal mean survival time for a triply periodic porous medium with a simply connected pore space at a porosity of 1/2 are achieved by the structure that globally minimizes the specific surface (63, 64). The verification of this conjecture remains an outstanding open question. This extremal problem falls in the general class of isoperimetric problems, which are notoriously difficult to solve. A prototypical isoperimetric example is Kelvin's problem: the determination of the space-filling arrangement of closed cells of equal volume that minimizes the surface area. Although it is believed that the Weaire-Phelan structure (65) is an excellent solution to Kelvin's problem, there is no proof that it is a globally optimal one. (The Weaire-Phelan structure uses two kinds of cells of equal volume: an irregular pentagonal dodecahedron and a tetrakaidecahedron with 2 hexagons and 12 pentagons, each face of which is slightly curved.) Our conjecture is also likely a difficult one to prove.

In this regard, it is noteworthy that an original goal of Jung et al. (66) was to show that the triply periodic surface with minimal specific surface s at porosity $\phi = 1/2$ is the Schwartz P surface. Although numerical simulations provided empirical evidence supporting this proposition, these authors (66) could not prove it rigorously. However, they were able to show that the Schwartz P, Schwartz D, and Schoen G minimal surfaces are local minima of the specific surface area s at fixed volume fraction $\phi = 1/2$. Thus, the question of the global optimality of the Schwartz P surface (i.e., minimal total interface surface area or specific surface s) is open for future investigation.

2.3. Photonic and Phononic Band Gaps

Recently, optimization techniques have been applied to design heterogeneous materials with photonic band gaps (PBGs). PBG materials are structures composed of two or more materials with different dielectric constants arranged in a spatial configuration that forbids the propagation of electromagnetic waves in a certain frequency range (67). These materials can be considered to be the photonic analog of electronic semiconductors, and as such they have found wide technological relevance (67–69).

Computing PBGs is computationally intensive because they require finding the eigenvalues associated with Maxwell's equations of electromagnetism. Thus, any optimization procedure to compute optimal PBGs is highly challenging, and full-blown topology optimization techniques are difficult to implement. Instead, such techniques have been used in combination with other optimization procedures to design two-dimensional materials with PBGs (see Reference 70 and references therein). It has been conjectured that the two-dimensional structure with the largest transverse magnetic (TM) polarization band gap consists of a triangular lattice of circular inclusions (70). A recent study has demonstrated that at low dielectric-contrast ratio there exist quasicrystal structures with larger band gaps (71). A photonic quasicrystal consists of two or more dielectric materials arranged in a quasiperiodic pattern with noncrystallographic symmetry that has a photonic band gap. However, it was shown in Reference 71 that at sufficiently high contrast the triangular lattice of circular inclusions conjectured in Reference 70 becomes optimal. Recently, a constrained optimization technique that employs a certain decoration of an underlying hyperuniform point pattern has been used with great success to design two-dimensional optimized materials with complete [both TM and transverse electric (TE)] polarization modes (72, 73). The topology optimization technique has also been applied to design heterogeneous materials with phononic PBG materials (74) that prevent elastic waves from propagating in certain frequency ranges.

3. RECONSTRUCTION TECHNIQUES

The reconstruction of realizations of disordered materials, such as liquids, glasses, and random heterogeneous materials, from a knowledge of limited microstructural information (lower-order correlation functions) is an intriguing inverse problem. Clearly, one can never reconstruct the original material perfectly, i.e., such reconstructions are nonunique. Thus, the objective here is not the same as that of data decompression algorithms that efficiently restore complete information, such as the gray scale of every pixel in an image.

The generation of realizations of heterogeneous materials with specified lower-order correlation functions can

1. shed light on the nature of the information contained in the various correlation functions that are employed;
2. ascertain whether the standard two-point correlation function, accessible experimentally via scattering, can accurately reproduce the material and, if not, what additional information is required to do so;
3. identify the class of microstructures that have exactly the same lower-order correlation functions but widely different effective properties;
4. probe the interesting issue of nonuniqueness of the generated realizations;
5. construct structures that correspond to specified correlation functions (termed the construction problem) and categorize classes of random media;

6. provide guidance in ascertaining the mathematical properties that physically realizable correlation functions must possess (1, 75–77); and
7. attempt three-dimensional reconstructions from slices or micrographs of the sample: a poor man's X-ray microtomography experiment.

The first reconstruction procedures applied to heterogeneous materials were based on thresholding Gaussian random fields. This approach to reconstruct random media originated with Joshi (78) and was extended by Adler (24) and Roberts & Teubner (79). This method is currently limited to the standard two-point correlation function and is not suitable for extension to non-Gaussian statistics.

3.1. Correlation Functions

Before discussing the optimization procedure to reconstruct or construct microstructures, we first introduce and define the various correlation functions that are targeted here. We focus on two-phase media, but the extension to multiple phases is straightforward.

Each realization of the two-phase random medium occupies some subset $\mathcal{V}$ of d-dimensional Euclidean space, i.e., $\mathcal{V} \in \mathbb{R}^d$. The region of space $\mathcal{V} \in \mathbb{R}^d$ of volume V is partitioned into two disjoint random sets or phases: phase 1, a region $\mathcal{V}_1$ of volume fraction φ_1, and phase 2, a region $\mathcal{V}_2$ of volume fraction ϕ_2 (see **Figure 1**). Let $\partial\mathcal{V}$ denote the surface or interface between $\mathcal{V}_1$ and $\mathcal{V}_2$. For a given realization, the indicator function $\mathcal{I}^{(i)}(\mathbf{x})$ for phase i for $\mathbf{x} \in \mathcal{V}$ is a random variable defined by

$$\mathcal{I}^{(i)}(\mathbf{x}) = \begin{cases} 1, & \text{if } \mathbf{x} \in \mathcal{V}_i, \\ 0, & \text{otherwise}, \end{cases} \tag{7.}$$

for $i = 1, 2$. Depending on the physical context, phase i can be a solid, fluid, or void characterized by some general tensor property. The indicator function $\mathcal{M}(\mathbf{x})$ for the interface is defined as

$$\mathcal{M}(\mathbf{x}) = |\nabla\mathcal{I}^{(1)}(\mathbf{x})| = |\nabla\mathcal{I}^{(2)}(\mathbf{x})| \tag{8.}$$

and therefore is a generalized function (e.g., a function involving Dirac delta functions) that is nonzero when $\mathbf{x}$ is on the interface.

In what follows, we define various statistical descriptors, the majority of which arise in structure/property relations (1).

3.1.1. *N*-point correlation functions.

The standard two-point correlation function is defined as

$$S_2^{(i)}(\mathbf{x}_1, \mathbf{x}_2) = \langle \mathcal{I}^{(i)}(\mathbf{x}_1)\mathcal{I}^{(i)}(\mathbf{x}_2)\rangle, \tag{9.}$$

where angular brackets denote an ensemble average. This function is the probability of finding two points $\mathbf{x}_1$ and $\mathbf{x}_2$ both in phase i. For statistically homogeneous and isotropic microstructures, which is the focus of the rest of this review article, two-point correlation functions will depend only on the distance $r \equiv |\mathbf{x}_1 - \mathbf{x}_2|$ between the points and hence $S_2^{(i)}(\mathbf{x}_1, \mathbf{x}_2) = S_2^{(i)}(r)$. Of course, when the two points coincide (i.e., $r = 0$), the two-point function must equal the volume fraction of phase i, i.e., $S_2^{(i)}(0) = \phi_i$. Henceforth, we drop the superscripted i and consider only the correlation functions for the phase of interest.

The n-point correlation is defined as one would expect (1):

$$S_n(\mathbf{x}_1, \mathbf{x}_2, \ldots, \mathbf{x}_n) = \langle \mathcal{I}(\mathbf{x}_1)\mathcal{I}(\mathbf{x}_2)\cdots\mathcal{I}(\mathbf{x}_n)\rangle. \tag{10.}$$

Theoretical representations of S_n have been obtained for nontrivial model microstructures of two-phase random heterogeneous materials (1, 80–82).

3.1.2. Surface correlation functions. The surface-void F_{sv} and surface-surface F_{ss} correlation functions are respectively defined as

$$F_{sv}(r) = \langle \mathcal{M}(\mathbf{x}_1)\mathcal{I}(\mathbf{x}_2)\rangle, \quad F_{ss}(r) = \langle \mathcal{M}(\mathbf{x}_1)\mathcal{M}(\mathbf{x}_2)\rangle, \tag{11.}$$

where $\mathcal{M}(\mathbf{x}) = |\nabla\mathcal{I}(\mathbf{x})|$ is the two-phase interface indicator function. By associating a finite thickness with the interface, F_{sv} and F_{ss} can be interpreted as, respectively, the probability of finding $\mathbf{x}_1$ in the dilated interface region and $\mathbf{x}_2$ in the void phase and the probability of finding both $\mathbf{x}_1$ and $\mathbf{x}_2$ in the dilated interface region but in the limit that the thickness tends to zero (1).

3.1.3. Lineal measures. The lineal-path function $L(r)$ is the probability that an entire line of length r lies in the phase of interest and thus contains a coarse level of connectedness information, albeit only along a lineal path (1, 83). The chord-length density function $p(r)$ gives the probability associated with finding a chord of length r in the phase of interest and is directly proportional to the second derivative of $L(r)$ (84). Chords are the line segments between the intersections of an infinitely long line with the two-phase interface.

3.1.4. Pore-size functions. The pore-size function $F(\delta)$ is related to the probability that a sphere of radius r lies entirely in the phase of interest (1) and therefore is the three-dimensional spherical version of the lineal measure L. The quantity $P(\delta) = -\partial F/\partial\delta$ is the pore-size probability density function, i.e., $P(\delta)d\delta$ is the probability that a randomly chosen point in the phase of interest lies at a distance between δ and $\delta + d\delta$ from the nearest point on the pore-solid interface $\partial\mathcal{V}$.

3.1.5. Two-point cluster function. The two-point cluster function $C_2(r)$ gives the probability of finding two points separated by a distance r in the same cluster of the phase of interest (85). A cluster of a phase is any topologically connected subset of that phase. The two-point cluster function can be measured experimentally using any appropriate three-dimensional imaging technique (e.g., tomography, confocal microscopy, or MRI) (1). That C_2 contains intrinsic three-dimensional topological information is to be contrasted with S_2, which can be obtained from a planar cross section of the heterogeneous material. In general, C_2 is expected to embody a much greater level of three-dimensional connectedness information than either L or F, but the degree to which this is true has only recently been demonstrated quantitatively (86).

3.2. Optimization Problem

Rintoul & Torquato (87) and Yeong & Torquato (88) proposed that reconstruction or construction problems can be posed as optimization problems. This is now a popular technique (89–92) because it is simple to implement, yields relatively robust solutions, and can incorporate any number and types of correlation functions in principle. A set of target correlation functions is prescribed on the basis of experiments, theoretical models, or some ansatz. Starting from some initial realization of the random medium, the method proceeds to find a realization by evolving the microstructure such that the calculated correlation functions best match the target functions. This is achieved by minimizing an error based upon the distance between the target and calculated correlation functions. The medium can be a dispersion of particles (87) or, more generally, a digitized image of a disordered material (88).

For simplicity, we introduce the problem for the case of digitized heterogeneous media here and consider for the moment a single correlation function at the two-point level for statistically isotropic two-phase media. [The generalization to multiple correlation functions for multiphase media is straightforward (87, 88).] It is desired to generate realizations of two-phase isotropic

media that have a target two-point correlation function $f_2(r)$ associated with the phase of interest, where r is the distance between the two points. Let $\hat{f}_2(r)$ be the corresponding function of the reconstructed digitized system (with periodic boundary conditions) at some intermediate time step. It is this system that we attempt to evolve toward $f_2(r)$ from an initial guess of the system realization. Again, for simplicity, we define a fictitious energy (or norm-2 error) E at any particular stage as

$$E = \sum_r [\hat{f}_2(r) - f_2(r)]^2, \qquad 12.$$

where the sum is over all discrete values of r.

Potential candidates for the two-point descriptors include the aforementioned ones: the standard two-point probability function $S_2(r)$, the surface-surface correlation function $F_{ss}(r)$, the surface-void correlation function $F_{sv}(r)$, the lineal-path function $L(r)$, the chord-length density function $p(r)$, the pore-size function $F(r)$, and the two-point cluster function $C_2(r)$.

3.3. Solution of Optimization Problem

The aforementioned optimization problem is very difficult to solve due to (*a*) the complicated nature of the objective function, which involves complex microstructural information in the form of correlation functions of the material, and (*b*) the combinatorial nature of the feasible set. Standard mathematical programming techniques are therefore most likely inefficient and likely to get trapped in local minima. In fact, the complexity and generality of the reconstruction problem make it difficult to devise deterministic algorithms of wide applicability. One therefore often resorts to heuristic techniques for global optimization, in particular, the simulated annealing method.

Simulated annealing has been applied successfully to many difficult combinatorial problems, including NP-hard ones such as the traveling-salesman problem. [NP-hard (nondeterministic polynomial time hard), in computational complexity theory, is a class of problems that are, roughly speaking, at least as hard as the hardest problems in NP.] The utility of the simulated annealing method stems from its simplicity—it requires only black-box cost function evaluations—and from its physically designed ability to escape local minima via accepting locally unfavorable configurations. In the method's simplest form, the states of two selected pixels of different phases are interchanged, automatically preserving the volume fraction of both phases. The change in the error (or energy) $\Delta E = E' - E$ between the two successive states is computed. This phase interchange is then accepted with some probability $p(\Delta E)$ that depends on ΔE. One reasonable choice is the Metropolis acceptance rule, i.e.,

$$p(\Delta E) = \begin{cases} 1, & \Delta E \leq 0, \\ \exp(-\Delta E/T), & \Delta E > 0, \end{cases} \qquad 13.$$

where T is a fictitious "temperature." The concept of finding the lowest-error (lowest-energy) state by simulated annealing is based on a well-known physical fact: If a system is heated to a high temperature T and then slowly cooled down to absolute zero, the system equilibrates to its ground state.

There are various ways of appreciably reducing computational time. For example, computational cost can be significantly lowered by using other stochastic optimization schemes such as the Great Deluge algorithm, which can be adjusted to accept only downhill energy changes, and the threshold acceptance algorithm (93). Further savings can be attained by developing strategies that exploit the fact that pixel interchanges are local, and thus one can reuse the correlation functions

measured in the previous time step instead of recomputing them fully at any step (88). Additional cost savings have been achieved by interchanging pixels only at the two-phase interface (1, 94).

3.4. Reconstructing Digitized Media

Lower-order correlation functions generally do not contain complete information and thus cannot be expected to yield perfect reconstructions. Of course, the judicious use of combinations of lower-order correlation functions can yield more accurate reconstructions than any single function alone. Yeong & Torquato (88, 95) clearly showed that the two-point function S_2 alone is not sufficient to reconstruct accurately random media. By also incorporating the lineal-path function L, they were able to obtain better reconstructions. They studied one-, two-, and three-dimensional digitized isotropic media. Each simulation began with an initial configuration of pixels (white for phase 1 and black for phase 2) in the random checkerboard arrangement at a prescribed volume fraction.

A two-dimensional example illustrating the insufficiency of S_2 in reconstructions is a target system of overlapping disks at a disk volume fraction of $\phi_2 = 0.5$; see **Figure 7*a***. Reconstructions that accurately match S_2 alone, L alone, or both S_2 and L are shown in **Figure 7**. The S_2 reconstruction is not very accurate; the cluster sizes are too large, and the system actually percolates. [Note that overlapping disks percolate at a disk area fraction of $\phi_2 \approx 0.68$ (1).] The L reconstruction does a better job than the S_2 reconstruction in capturing the clustering behavior. However, the hybrid ($S_2 + L$) reconstruction is the best. Note that both S_2 and L were sampled along two orthogonal

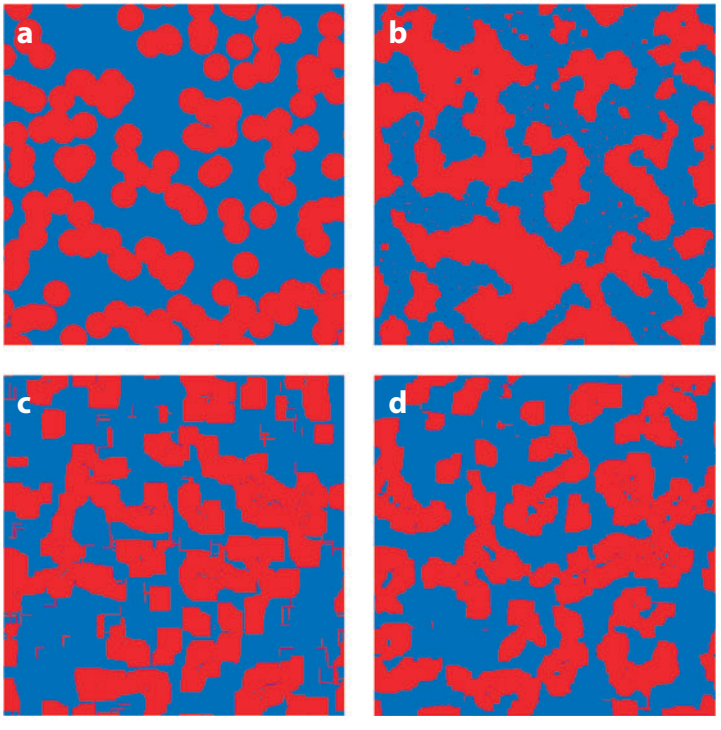

Figure 7

(*a*) Target system: a realization of random overlapping disks. System size = 400 × 400 pixels, disk diameter = 31 pixels, and volume fraction $\phi_2 = 0.5$. (*b*) S_2 reconstruction. (*c*) Corresponding L reconstruction. (*d*) Corresponding hybrid ($S_2 + L$) reconstruction. Adapted from Yeong & Torquato (88).

directions to save computational time. This time-saving step should be implemented only for isotropic media, provided that there is no appreciable short-range order; otherwise, unwanted anisotropy results (93, 96). However, this artificial anisotropy can be reduced by optimizing along additional selected directions (97) or along all directions (86, 98).

3.4.1. Superior two-point statistical descriptor. It is now well established that $S_2(\mathbf{r})$ is not sufficient information to get an accurate rendition of the original microstructure (88, 93–95, 98). In other words, the ground states when only S_2 is incorporated in the energy (Equation 12) are highly degenerate due to the nonuniqueness of the information content of this two-point function, which is clearly illustrated by the subsequent examples in the paper.

Therefore, an outstanding fundamental problem is to identify other two-point correlation functions that both can be manageably measured and yet reflect nontrivial higher-order structural information about the media. Presumably, incorporation of such a two-point function in reconstruction methods would yield highly accurate renditions of the media. Recently, the inverse methodology of Yeong & Torquato (88) was used to determine the amount of structural information that is embodied in a set of targeted correlation functions by quantifying the extent to which the original structure can be accurately reconstructed by employing those target functions (86). The accuracy of a reconstruction was quantified by measuring unconstrained (untargeted) correlation functions and comparing them to those of the original medium. It was shown that a superior two-point signature of random media is the two-point cluster function $C_2(\mathbf{r})$ (85) because it contains not only appreciably more information than S_2 but more information than a variety of other "two-point" quantities, including the surface-surface correlation function F_{ss}, the surface-void correlation function F_{sv}, the pore-size function F, lineal-path function L, and the chord-length density function p.

Target random media were drawn from materials science, cosmology, and granular media, among other fields. Here we describe just two examples that were considered: a concrete microstructure and a dense sphere packing.

The wide range of structural features in concrete, from nanometer-sized pores to centimeter-sized aggregates, makes it a wonderful example of a multiscale microstructure (99). **Figure 8*a*** shows a binarized digitized image of a concrete sample cross section. The original image was thresholded so that the blue phase represents the stones and the lighter gray phase is the cement paste. The stone phase is characterized by a dense dispersion of particles of various sizes: a nontrivial situation to reconstruct. Using S_2 alone overestimates clustering in the system and indeed incorrectly yields a percolating particle phase. Thus, although S_2 of the reconstruction matches the target one with very small error, such information is insufficient to get a good reconstruction. Incorporating both S_2 and the surface-surface function F_{ss} leads to a better rendition of the target system, but the reconstruction still overestimates the degree of clustering. In contrast, incorporating C_2 yields an excellent reconstruction in that the stone phase clearly appears as a particle dispersion with a size distribution that closely matches that of the target structure. Jiao et al. (86) quantitatively tested the accuracy of the reconstructions by measuring unconstrained correlation functions and comparing them to the corresponding quantities of the target system. They chose to compute the unconstrained lineal-path function L. **Figure 8*e*** reveals that the lineal-path function of the reconstruction that incorporates C_2 matches the target function L well and that it is appreciably more accurate than the other reconstructions.

As an application of their methodology to three dimensions, Jiao et al. (86) reconstructed a digitized realization of an equilibrium distribution of equal-sized hard spheres, as shown in **Figure 9*a***. This packing was generated using the standard Metropolis Monte Carlo technique

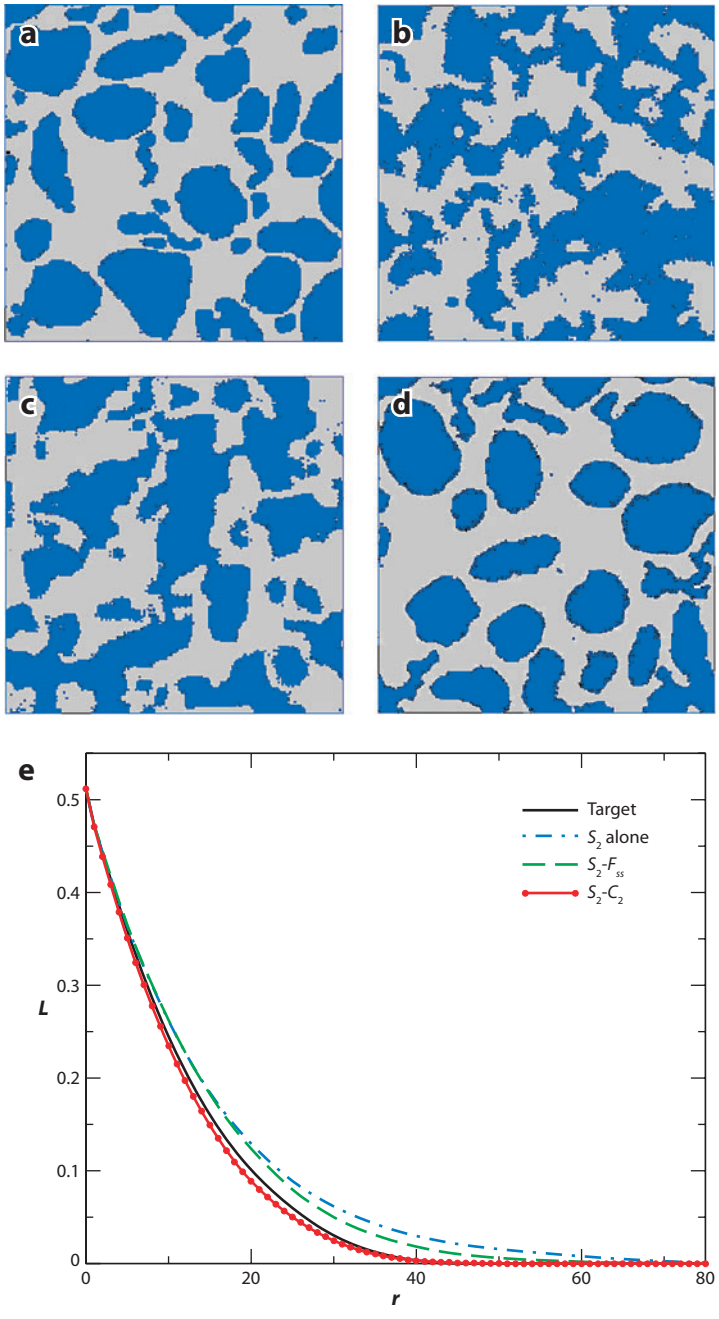

Figure 8

(*a*) Target system: a binarized image of a cross section of concrete, as taken from Reference 86. The linear size of the digitized heterogeneous material is $N_L = 170$ pixels. (*b*) S_2-alone reconstruction. (*c*) S_2-F_{ss} hybrid reconstruction. (*d*) S_2-C_2 hybrid reconstruction. All the reconstructions are associated with a final energy (error) $E \sim 10^{-8}$. (*e*) The unconstrained lineal-path function L of the reconstructions and the target image. Pixel size supplies the unit for the distance r.

Figure 9

(*a*) Target system: a digitized realization of a hard-sphere packing in which the spheres occupy 44.6% of space, as taken from Reference 86. The linear size of the digitized heterogeneous material is $N_L = 100$ pixels. (*b*) S_2-alone reconstruction. (*c*) S_2-F reconstruction. (*d*) S_2-C_2 hybrid reconstruction. All the reconstructions are associated with a final energy (error) $E \sim 10^{-11}$. (*e*) The (unconstrained) lineal-path function sampled from target and reconstructed realizations. Pixel size supplies the unit for the distance r.

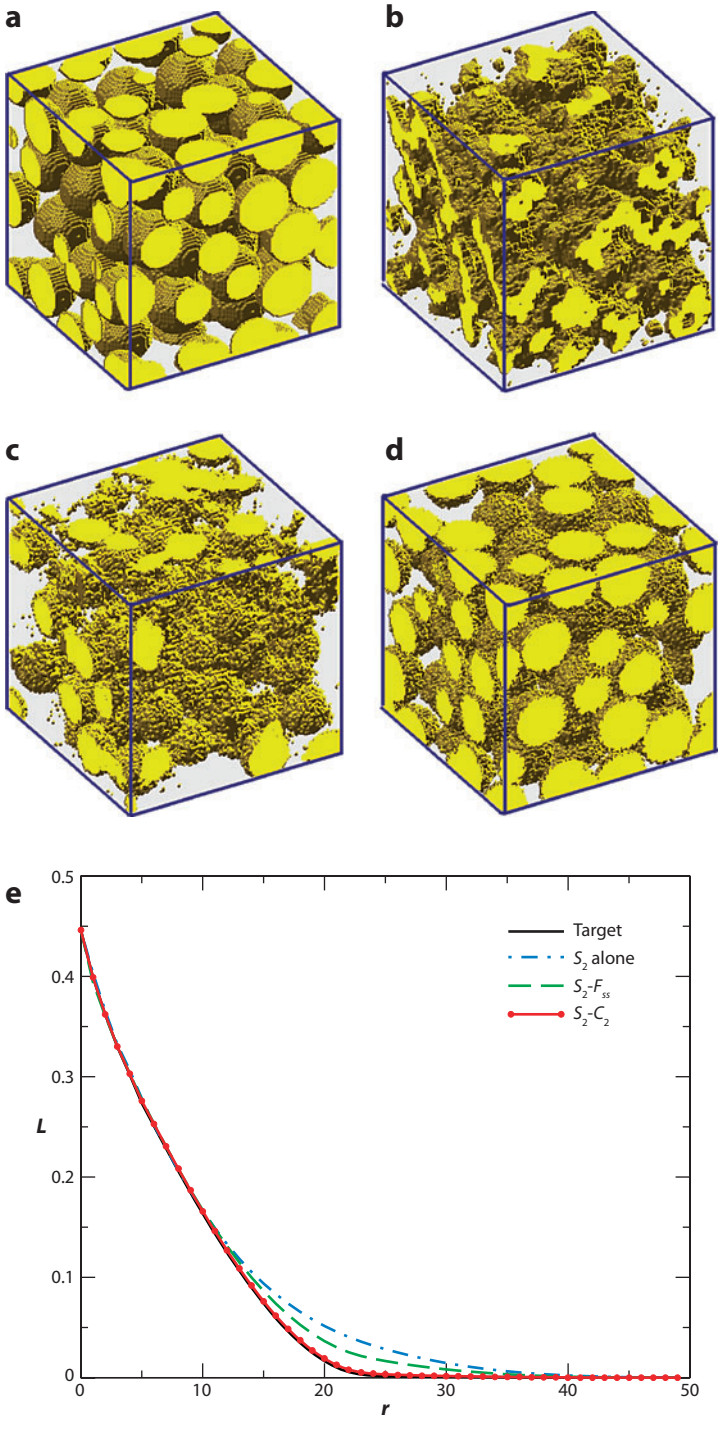

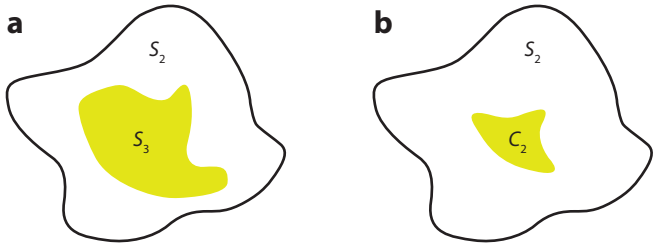

Figure 10

The set of all microstructures associated with a particular S_2 is schematically shown as the region enclosed by the solid black contour in both panels *a* and *b* (86). (*a*) The shaded region shows the set of all microstructures associated with the same S_2 and S_3. (*b*) The yellow, more restrictive region shows the set of all microstructures associated with the same S_2 and C_2.

for a canonical ensemble of hard spheres in a cubical box under periodic boundary conditions (1). A visual comparison of the hybrid reconstruction involving the two-point cluster function reveals that it accurately yields a dispersion of well-defined spherical inclusions of the same size, in contrast to the S_2 reconstruction, which again grossly overestimates clustering of the sphere phase. In contrast to the previous example, here the pore-size function F (not the surface correlation functions) is incorporated in one of the reconstructions. Although the reconstruction incorporating F provides improvement over the rendition on the S_2-alone reconstruction, it is still inferior to the S_2-C_2 reconstruction in reproducing both the size and shape of the sphere phase. The accuracy of the S_2-C_2 hybrid reconstruction can also be seen by comparing the unconstrained lineal-path function L of the target system to those L functions of the reconstructed media (see **Figure 9*e***).

In summary, for all the examples studied in Reference 86, reconstructions that included the two-point cluster function C_2 were always found to be significantly more accurate than those involving any of the combinations of pairs of the other functions. More precisely, the incorporation of C_2 significantly reduces the number of compatible microstructures as compared with the compatible microstructures consistent with the same three-point function S_3, which is schematically indicated in **Figure 10**.

3.5. Constructing Digitized Media

The optimization method can be used in the construction mode to find the specific structures that realize a specified set of correlation functions. An interesting question in this regard is the following: Is any hypothesized correlation function physically realizable, or must the function satisfy certain conditions? Not all hypothetical correlation functions are physically realizable. For example, what are the existence conditions for a valid (i.e., physically realizable) autocovariance function $\chi(\mathbf{r}) \equiv S_2(\mathbf{r}) - \phi_1^2$ for statistically homogeneous two-phase media? It is well-known that there are certain nonnegativity conditions involving the spectral representation of the autocovariance $\chi(\mathbf{r})$ that must be obeyed (1, 75–77). However, it is not well-known that these nonnegativity conditions are necessary but not sufficient conditions that a valid autocovariance $\chi(\mathbf{r})$ of a statistically homogeneous two-phase random medium (i.e., a binary stochastic spatial process) must meet. The complete characterization of the existence conditions is a very difficult problem. Suffice it to say that the algorithm in the construction mode can be used to provide guidance on the development of the mathematical conditions that a valid autocovariance $\chi(\mathbf{r})$ must obey.

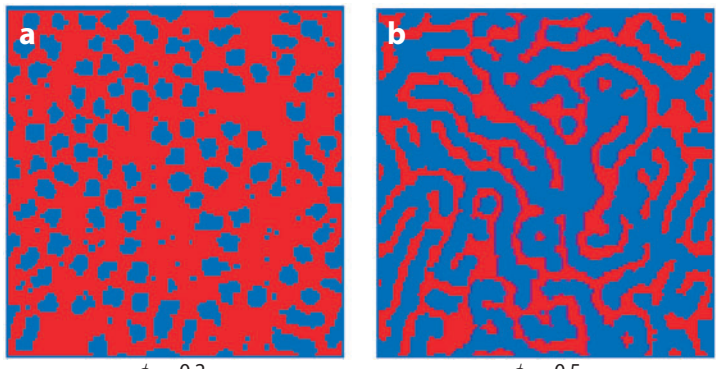

Figure 11

Structures corresponding to the target correlation function given by Equation 14 for $\phi_2 = 0.2$ and $\phi_2 = 0.5$. Here $a = 32$ pixels and $b = 8$ pixels.

Cule & Torquato (93) considered the construction of realizations having the following autocovariance function:

$$\frac{S_2(r) - \phi_1^2}{\phi_1 \phi_2} = e^{-r/a} \frac{\sin(qr)}{qr}, \qquad 14.$$

where $q = 2\pi/b$ and the positive parameter b is a characteristic length that controls oscillations in the term $\sin(qr)/(qr)$, which also decays with increasing r. This function possesses phase-inversion symmetry (1) and exhibits a considerable degree of short-range order; it generalizes the purely exponentially decaying function studied by Debye et al. (100). This function satisfies the nonnegativity condition on the spectral function but may not satisfy the binary conditions, depending on the values of a, b, and ϕ_1 (75). Two structures possessing the correlation function (14) are shown in **Figure 11** for $\phi_2 = 0.2$ and $\phi_2 = 0.5$, in which $a = 32$ pixels and $b = 8$ pixels. For these sets of parameters, all the aforementioned necessary conditions on the function are met. At $\phi_2 = 0.2$, the system resembles a dilute particle suspension with particle diameters of order b. At $\phi_2 = 0.5$, the resulting pattern is labyrinthine such that the characteristic sizes of the patches and walls are of order a and order b, respectively. Note that $S_2(r)$ was sampled in all directions during the annealing process.

To what extent can information extracted from two-dimensional cuts through a three-dimensional isotropic medium, such as S_2 and L, be employed to reproduce intrinsic three-dimensional information, such as connectedness? This question was studied for a Fontainebleau sandstone for which we know the full three-dimensional structure via X-ray microtomography (95). **Figure 12** shows the three-dimensional reconstruction that results by using a single slice of the sample and matching both S_2 and L. The reconstructions accurately reproduce certain three-dimensional properties of the pore space, such as the pore-size functions, the mean survival time of a Brownian particle, and the fluid permeability. The degree of connectedness of the pore space also compares remarkably well with the actual sandstone, although this is not always the case (101).

3.6. Reconstructing Many-Particle Systems

The aforementioned reconstruction/construction algorithm was applied originally to reconstruct realizations of many-particle systems (87). For statistically homogeneous systems consisting of

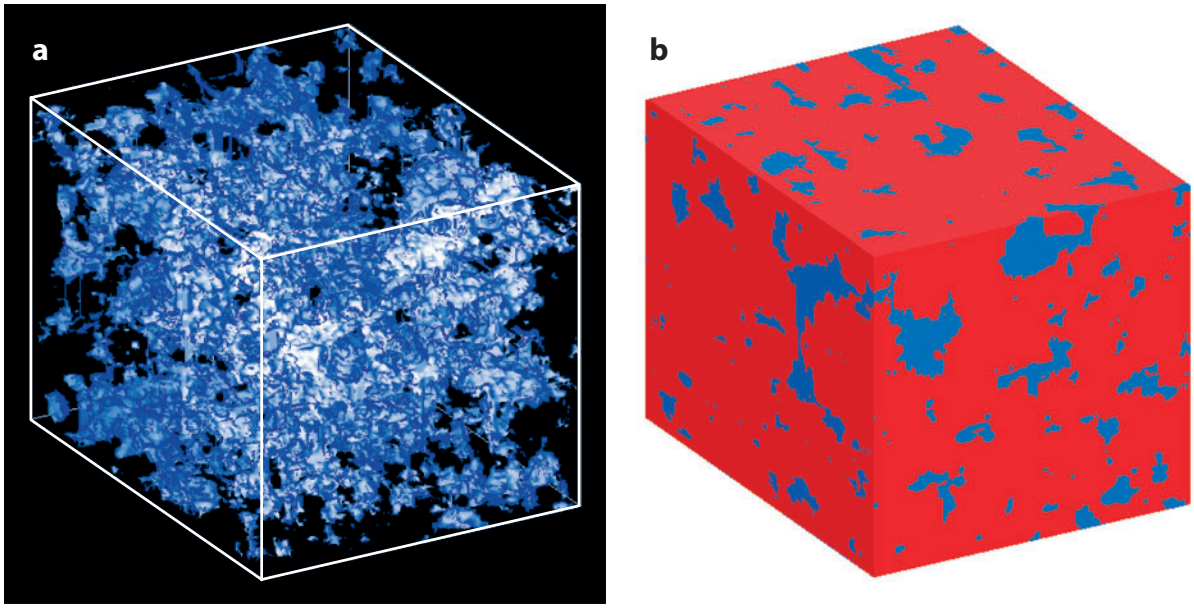

Figure 12

Hybrid reconstruction of a sandstone [described in Torquato (1)] using both S_2 and L obtained from a single slice. System size is $128 \times 128 \times 128$ pixels. (*a*) Pore space is the blue region, and the grain phase is transparent. (*b*) Three-dimensional perspective of the surface cuts, where the blue region is the pore phase and the red region is the grain phase (1).

identical spherical particles in a large volume at number density ρ, the most natural statistical descriptor is the n-particle correlation function $g_n(\mathbf{r}_1, \mathbf{r}_2, \ldots, \mathbf{r}_n)$, which is proportional to the probability density for simultaneously finding n particles at locations $\mathbf{r}_1, \mathbf{r}_2, \ldots, \mathbf{r}_n$ within the system (1, 102). The pair correlation function g_2 is usually the quantity of primary interest and, if the system is additionally isotropic, depends only upon the distance $r = |\mathbf{r}_2 - \mathbf{r}_1|$ between pair positions. The pair correlation function can be ascertained from scattering experiments, which makes it a natural candidate for the reconstruction of a real many-particle system.

The hard-sphere system in which pairs of particles interact only with an infinite repulsion when they overlap is one of the simplest interacting particle systems (1). Importantly, the impenetrability constraint does not uniquely specify the statistical ensemble. The hard-sphere system can be in thermal equilibrium or in one of the infinitely many nonequilibrium states, such as the random sequential addition (or adsorption) (RSA) process that is produced by randomly, irreversibly, and sequentially placing nonoverlapping objects into a volume (1). Whereas particles in equilibrium have thermal motion such that they sample the configuration space uniformly, particles in an RSA process do not sample the configuration space uniformly because their positions are forever frozen (i.e., do not diffuse) after they have been placed into the system. The geometrical blocking effects and the irreversible nature of the process result in structures that are distinctly different from corresponding equilibrium configurations, except for low densities. The saturation limit (the final state of this process whereby no particles can be added) occurs at a particle volume fraction or packing fraction $\phi \equiv \phi_2 \approx 0.55$ in two dimensions (1).

Two-dimensional RSA circular disk systems have been reconstructed using a target pair correlation function $g_2(r)$ (87). Thus, the target function in Equation 12 is taken to be g_2. The initial configuration was 5000 disks in equilibrium. **Figure 13** shows a realization of the RSA system near

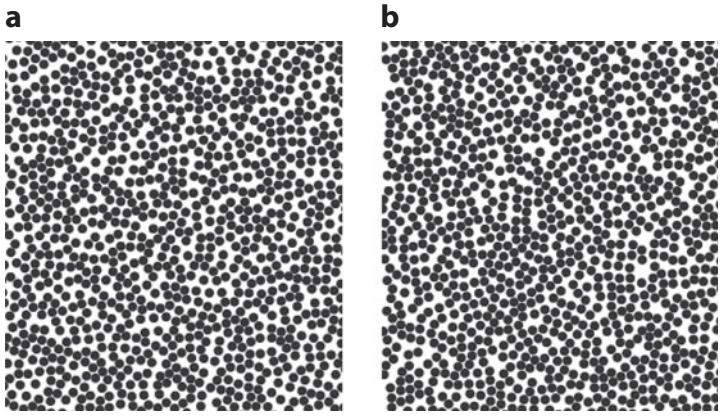

Figure 13

(*a*) A portion of a sample random sequential addition (or adsorption) (RSA) system at a packing fraction $\phi = 0.543$, which is in the near vicinity of the saturation state. (*b*) A portion of the reconstructed RSA system at $\phi = 0.543$ (87).

its saturation state at a particle volume fraction $\phi = 0.543$ (**Figure 13*a***) and the reconstructed system at the same particle volume fraction (**Figure 13*b***). As a quantitative comparison of how the original and reconstructed systems matched, it was found that the corresponding pore-size functions (1) were similar. This conclusion gives one confidence that a reasonable facsimile of the actual structure can be produced from the pair correlation function for a class of many-particle systems in which there is not significant clustering of the particles. However, it is not sufficient to reconstruct particulate systems in which there is significant clustering (87). For such systems, recent work (86) suggests that the pair-connectedness function P_2 [i.e., the connectedness contribution to g_2 (1)] plus the pair correlation function g_2 contain considerably more information than that contained in the combination of g_2 and the three-particle correlation function g_3.

3.7. Constructing Many-Particle Systems and the Realizability Problem

An important application of the stochastic optimization technique in the construction mode involves a fascinating open question concerned with whether a prescribed hypothetical pair correlation function $g_2(\mathbf{r})$ actually represents the pair correlation of some many-particle configuration at number density $\rho > 0$. This is termed the realizability problem (103, 104). We know of several necessary conditions that must be satisfied by such a hypothetical function, including nonnegativity of $g_2(\mathbf{r})$ and its associated structure factor

$$S(k) = 1 + \rho \int_{\mathbb{R}^d} \exp(-i\mathbf{k} \cdot \mathbf{r})[g_2(r) - 1]d\mathbf{r} \qquad 15.$$

as well as constraints on implied local density fluctuations (105). A positive g_2 at a positive ρ must satisfy an uncountable number of necessary and sufficient conditions for it to correspond to a realizable point process (106, 107). However, these conditions are very difficult (or, more likely, impossible) to check for arbitrary dimension. In other words, given ρ and g_2, it is difficult to ascertain if there are some higher-order functions $g_3, g_4, \ldots$ for which these one- and two-particle correlation functions hold.

To explore and gain insight into the basic statistical geometric features of random sphere packings, the notion of a g_2-invariant process was introduced (103). A g_2-invariant process is one in which a given nonnegative pair correlation $g_2(\mathbf{r})$ function remains invariant as density varies for

all **r** over the range of packing fractions

$$0 \leq \phi \leq \phi_*. \qquad 16.$$

The terminal packing fraction ϕ_* is the maximum achievable value for the g_2-invariant process subject to satisfaction of the known necessary conditions for the pair correlation function. The determination of the terminal packing fraction for various forms of g_2 that putatively correspond to a sphere packing has been solved using numerical and analytical optimization techniques (103, 108–111).

To test whether such g_2s at terminal packing fraction ϕ_* are indeed realizable by sphere packings, the aforementioned stochastic optimization technique has been employed to construct packings with targeted lower-order correlation functions (112, 113). In a construction algorithm, an initial configuration of particles evolves such that the final configuration possesses the targeted g_2 up to some cutoff distance.

For the elementary unit step-function pair correlation function

$$g_2(r) = \Theta(r - D), \qquad 17.$$

previous theoretical work (114) indicated that this function is achievable by hard-sphere configurations in d dimensions up to a terminal packing fraction $\phi_* = 2^{-d}$. Here D is the hard-sphere diameter, and $\Theta(x)$ is the unit step function (equal to zero for negative x and unity otherwise). To test whether the unit step g_2 is actually achievable by hard spheres for nonzero densities, the aforementioned stochastic optimization procedure was applied in the construction mode. Numerical calculations for $d = 1$ and $d = 2$ confirmed that the step-function g_2 is indeed realizable up to the terminal packing fraction (112). **Figure 14** compares an equilibrium hard-disk configuration at $\phi = 0.2$ with a corresponding annealed reconstructed step-function system.

For example, for the case of d-dimensional packing of congruent spheres of diameter D in which the pair correlation function is taken to be

$$g_2(r) = \frac{Z}{\rho s_1(r)}\delta(r - D) + \Theta(r - D), \qquad 18.$$

where Z represents the average contact value per sphere and $s_1(r) = d\pi^{d/2}r^{d-1}/\Gamma(1 + d/2)$ is the surface area of a d-dimensional sphere (103), the terminal packing fraction ϕ_* [the fraction of space covered by the spheres, equal to $rho_* v_1(D/2)$] and the associated average contact number

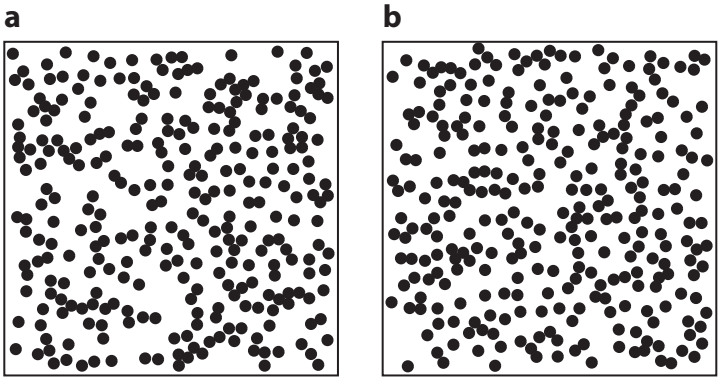

Figure 14

Configurations of 289 particles for $\phi_2 = 0.2$ in two dimensions (112). The equilibrium hard-disk system (*a*) shows more clustering and larger pores than does the annealed reconstructed step-function system (*b*).

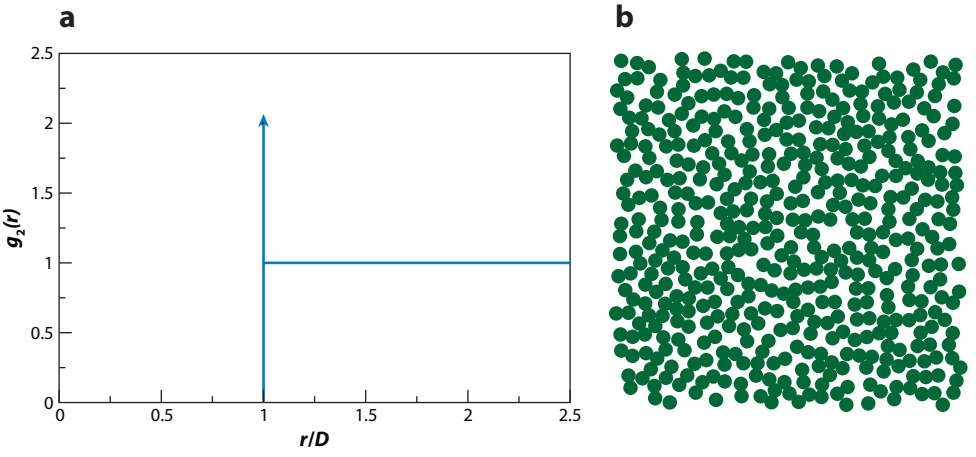

Figure 15

(*a*) Graph of the target pair correlation function $g_2(r)$: Dirac δ function plus a step function. (*b*) A two-dimensional configuration of 500 particles that realizes this targeted form for $g_2(r)$ up to a dimensionless distance of $r/D = 2.5$, as adapted from Reference 113. The configuration consists of only dimers at the terminal packing fraction $\phi_* = 0.5$ with an average contact value $Z = 1.0$.

Z_* are given by

$$\phi_* = \frac{d+2}{2^{d+1}}, \quad Z_* = \frac{d}{2}. \tag{19.}$$

Numerical evidence suggests that such a pair correlation is achieved by a single sphere-packing configuration for any $d \geq 2$ (113). Such a pair correlation function (**Figure 15**) shows a realization of such a packing in two dimensions. Of course, in any simulation, pair distances must binned and sampled up to some cutoff distance. For a sufficiently large system, the targeted correlation for a single configuration approaches that of one obtained from an ensemble of configurations by ergodicity.

Elsewhere, so-called iso-g_2 processes were studied in the equilibrium regime. These consist of a sequence of equilibrium many-body systems that have different number densities but share, at a given temperature, the same target pair correlation function. In other words, in these processes, density-dependent interactions identically cancel the usual density variation of many-body pair correlation functions (114–116). Target pair correlation functions studied include the unit step function as well as the zero-density limit of the square-well potential for which $g_2(r) = \exp[-\beta\varphi(r)]$, where β represents inverse temperature and φ of r is the pair potential. Formal density expansions for effective pair potentials were derived with this iso-g_2 property, showing how successive terms in that expansion can be determined iteratively. Explicit results through second-density order were obtained for two types of target pair correlation functions, and the conditions under which realizability can be attained were explored (116).

Because the realizability problem is far from being solved, it remains an active area of research. For example, it has been conjectured that any radial, nonnegative pair correlation function characterized by a hard core, which decays sufficiently rapidly to unity, is realizable by a translationally invariant disordered sphere packing in d-dimensional Euclidean space for asymptotically large d if and only if $S(k) \geq 0$ (117). Although there is mounting evidence to support this conjecture (108, 110, 117), which implies that the densest sphere packings in sufficiently high dimensions are counterintuitively disordered rather than ordered, its proof is a great challenge.

4. SUMMARY

Optimization methods provide a systematic means of designing heterogeneous materials with desired bulk properties and microstructures (1, 118). Combining such modeling techniques with novel synthesis and fabrication methodologies may make optimal design of real materials a reality in the future. The topology optimization technique and the stochastic reconstruction (construction) method address only a small subset of optimization issues of importance in materials science, but the results that are beginning to emerge from these relatively new methods bode well for progress in the future. Indeed, recent inverse statistical-mechanical methodologies have been devised to optimize interaction potentials in soft-matter systems (e.g., colloids and polymers) such that they spontaneously self-assemble into stable target structures (119).

DISCLOSURE STATEMENT

The author is not aware of any affiliations, memberships, funding, or financial holdings that might be perceived as affecting the objectivity of this review.

ACKNOWLEDGMENTS

It is with deep gratitude that I acknowledge my numerous collaborators over the past decade and a half, without whom this review article would not have been possible. This work has been supported by the Office of Basic Energy Sciences at the U.S. Department of Energy and the Petroleum Research Fund administered by the American Chemical Society.

LITERATURE CITED

1. Torquato S. 2002. *Random Heterogeneous Materials: Microstructure and Macroscopic Properties*. New York: Springer-Verlag
2. Maxwell JC. 1873. *Treatise on Electricity and Magnetism*. Oxford, UK: Clarendon Press
3. Rayleigh L. 1892. On the influence of obstacles arranged in a rectangular order upon the properties of medium. *Philos. Mag.* 34:481–502
4. Einstein A. 1906. Eine neue Bestimmung der Moleküldimensionen. *Ann. Phys.* 19:289–306
5. Christensen RM. 1979. *Mechanics of Composite Materials*. New York: Wiley
6. Jikov VV, Kozlov SM, Olenik OA. 1994. *Homogenization of Differential Operators and Integral Functionals*. Berlin: Springer-Verlag
7. Cherkaev AV. 2000. *Variational Methods for Structural Optimization*. New York: Springer-Verlag
8. Torquato S. 2000. Modeling of physical properties of composite materials. *Int. J. Solids Struct.* 37:411–22
9. Milton GW. 2002. *The Theory of Composites*. Cambridge, UK: Cambridge Univ. Press
10. Sahimi M. 2003. *Heterogeneous Materials I: Linear Transport and Optical Properties*. New York: Springer-Verlag
11. Hashin Z, Shtrikman S. 1962. A variational approach to the theory of the effective magnetic permeability of multiphase materials. *J. Appl. Phys.* 33:3125–31
12. McKenzie DR, McPhedran RC, Derrick GH. 1978. The conductivity of lattices of spheres. II. The body centered and face centered cubic lattices. *Proc. R. Soc. London Ser. A* 362:211–32
13. Bensoussan A, Lions JL, Papanicolaou G. 1978. *Asymptotic Analysis for Periodic Structures*. Amsterdam: North Holland
14. Milton GW. 1980. Bounds on the complex dielectric constant of a composite material. *Appl. Phys. Lett.* 37:300–2
15. Milton GW, Phan-Thien N. 1982. New bounds on effective elastic moduli of two-component materials. *Proc. R. Soc. London Ser. A* 380:305–31
16. Sheng P, Zhou MY. 1988. Dynamic permeability in porous media. *Phys. Rev. Lett.* 61:1591–94

17. Kohn RV, Lipton R. 1988. Optimal bounds for the effective energy of a mixture of isotropic, incompressible elastic materials. *Arch. Ration. Mech. Anal.* 102:331–50
18. Gibiansky LV, Torquato S. 1995. Geometrical-parameter bounds on effective moduli of composites. *J. Mech. Phys. Solids* 43:1587–613
19. Torquato S. 1997. Effective stiffness tensor of composite media. I. Exact series expansions. *J. Mech. Phys. Solids* 45:1421–48
20. Torquato S, Pham DC. 2004. Optimal bounds on the trapping constant and permeability of porous media. *Phys. Rev. Lett.* 92:255505
21. Rechtsman MC, Torquato S. 2008. Effective dielectric tensor for electromagnetic wave propagation in random media. *J. Appl. Phys.* 103:084901
22. Lee SB, Kim IC, Miller CA, Torquato S. 1989. Random-walk simulation of diffusion-controlled processes among static traps. *Phys. Rev. B* 39:11833–39
23. Kim IC, Torquato S. 1991. Effective conductivity of suspensions of hard spheres by Brownian motion simulation. *J. Appl. Phys.* 69:2280–89
24. Adler PM. 1992. *Porous Media—Geometry and Transports*. Boston: Butterworth-Heinemann
25. Eischen JW, Torquato S. 1993. Determining elastic behavior of composites by the boundary element method. *J. Appl. Phys.* 74:159–70
26. Helsing J. 1994. Bounds on the shear modulus of composites by interface integral methods. *J. Mech. Phys. Solids* 42:1123–38
27. Greengard L, Moura M. 1994. On the numerical evaluation of the electrostatic fields in composite materials. *Acta Numerica* 3:379–410
28. Garboczi EJ, Day AR. 1995. Algorithm for computing the effective linear elastic properties of heterogeneous materials: three-dimensional results for composites with equal Poisson ratios. *J. Mech. Phys. Solids* 43:1349–62
29. Cheng H, Greengard L. 1997. On the numerical evaluation of electrostatic fields in dense random dispersions of cylinders. *J. Comput. Phys.* 136:629–39
30. Moulinec H, Suquet P. 1998. A numerical method for computing the overall response of nonlinear composites with complex microstructure. *Comput. Meth. Appl. Mech. Eng.* 157:69–94
31. Eyre DJ, Milton GW. 1999. A fast numerical scheme for computing the response of composites using grid refinement. *Euro. Phys. J.* 6:41–47
32. Martys NS, Hagedorn JG. 2002. Multiscale modeling of fluid transport in heterogeneous materials using discrete Boltzmann methods. *Mater. Struct.* 35:650–59
33. Bendsøe MP, Kikuchi N. 1988. Generating optimal topologies in structural design using a homogenization method. *Comput. Methods Appl. Mech. Eng.* 71:197–224
34. Sigmund O, Torquato S. 1997. Design of materials with extreme thermal expansion using a three-phase topology optimization method. *J. Mech. Phys. Solids* 45:1037–67
35. Sigmund O, Torquato S, Aksay IA. 1998. On the design of 1-3 piezocomposites using topology optimization. *J. Mater. Res.* 13:1038–48
36. Bendsøe MP. 1995. *Optimization of Structural Topology, Shape and Material*. Berlin: Springer-Verlag
37. Hyun S, Torquato S. 2001. Designing composite microstructures with targeted properties. *J. Mater. Res.* 16:280–85
38. Torquato S, Hyun S, Donev A. 2002. Multifunctional composites: optimizing microstructures for simultaneous transport of heat and electricity. *Phys. Rev. Lett.* 89:266601
39. Torquato S, Hyun S, Donev A. 2003. Optimal design of manufacturable three-dimensional composites with multifuctional characteristics. *J. Appl. Phys.* 94:5748–55
40. Bendsøe MP, Sigmund O. 2003. *Topology Optimization*. Berlin: Springer-Verlag
41. Bergman DJ. 1978. The dielectric constant of a composite material—a problem in classical physics. *Phys. Rep. C* 43:377–407
42. Milton GW. 1981. Bounds on the complex permittivity of a two-component composite material. *J. Appl. Phys.* 52:5286–93
43. Avellaneda M, Cherkaev AV, Lurie KA, Milton GW. 1988. On the effective conductivity of polycrystals and a three-dimensional phase-interchange inequality. *J. Appl. Phys.* 63:4989–5003

44. Torquato S. 1990. Relationship between permeability and diffusion-controlled trapping constant of porous media. *Phys. Rev. Lett.* 64:2644–46
45. Torquato S, Avellaneda M. 1991. Diffusion and reaction in heterogeneous media: pore size distribution, relaxation times, and mean survival time. *J. Chem. Phys.* 95:6477–89
46. Avellaneda M, Torquato S. 1991. Rigorous link between fluid permeability, electrical conductivity, and relaxation times for transport in porous media. *Phys. Fluids A* 3:2529–40
47. Gibiansky LV, Torquato S. 1998. Rigorous connection between physical properties of porous rocks. *J. Geophys. Res.* 103:23911–23
48. Milton GW. 1984. Correlation of the electromagnetic and elastic properties of composites and microgeometries corresponding with effective medium approximations. In *Physics and Chemistry of Porous Media*, ed. DL Johnson, PN Sen, pp. 66–77. New York: AIP
49. Gibiansky LV, Torquato S. 1993. Link between the conductivity and elastic moduli of composite materials. *Phys. Rev. Lett.* 71:2927–30
50. Gibiansky LV, Torquato S. 1995. Rigorous link between the conductivity and elastic moduli of fibre-reinforced composite materials. *Philos. Trans. R. Soc. London Ser. A* 353:243–78
51. Gibiansky LV, Torquato S. 1996. Connection between the conductivity and bulk modulus of isotropic composite materials. *Proc. R. Soc. London Ser. A* 452:253–83
52. Torquato S, Hyun S. 2001. Effective-medium approximation for composite media: realizable single-scale dispersions. *J. Appl. Phys.* 89:1725–29
53. Hyun S, Torquato S. 2002. Optimal and manufacturable two-dimensional, kagomé-like cellular solids. *J. Mater. Res.* 17:137–44
54. Zohdi T. 2003. Genetic design of solids possessing a random-particulate microstructure. *Philos. Trans. R. Soc. London Ser. A* 361:1021–43
55. Van Tasell PR, Viot P. 1997. An exactly solvable continuum model of mutlilayer irreversible adsorption. *Europhys. Lett.* 40:293–98
56. Larsen UD, Sigmund O, Bouwstra S. 1997. Design and fabrication of compliant mechanisms and material structures with negative Poisson's ratio. *J. Microelectromech. Syst.* 6:99–106
57. Gibiansky LV, Torquato S. 1997. Thermal expansion of isotropic multiphase composites and polycrystals. *J. Mech. Phys. Solids* 45:1223–52
58. Gibiansky LV, Torquato S. 1997. Optimal design of 1-3 composite piezoelectrics. *Struct. Optim.* 13:23–28
59. Gibiansky LV, Torquato S. 1997. On the use of homogenization theory to design optimal piezocomposites for hydrophone applications. *J. Mech. Phys. Solids* 45:689–708
60. Gibiansky LV, Torquato S. 1999. Matrix laminates: realizable approximations for the effective moduli of piezoelectric composites. *J. Mater. Res.* 14:49–63
61. Milton GW. 1987. Multicomponent composites, electrical networks and new types of continued fractions. I and II. *Commun. Math. Phys.* 111:281–372
62. Torquato S, Donev A. 2004. Minimal surfaces and multifunctionality. *Proc. R. Soc. London Ser. A* 460:1849–56
63. Jung Y, Torquato S. 2005. Fluid permeabilities of triply periodic minimal surfaces. *Phys. Rev. E* 92:255505
64. Gevertz JL, Torquato S. 2009. Mean survivial times of absorbing triply periodic minimal surfaces. *Phys. Rev. E* 80:011102
65. Weaire D, Phelan R. 1994. A counterexample to Kelvin's conjecture on minimal surfaces. *Philos. Mag. Lett.* 69:107–10
66. Jung Y, Chu KT, Torquato S. 2007. A variational level set approach for surface area minimization of triply periodic media. *J. Comput. Phys.* 223:711–30
67. Joannopoulos JD, Johnson SG, Winn JN, Meade RD. 2008. *Photonic Crystals: Molding the Flow of Light*. Princeton, NJ: Princeton Univ. Press. 2nd ed.
68. Yaglom AM. 1987. *Correlation Theory of Stationary and Related Functions. I. Basic Results*. New York: Springer-Verlag
69. John S. 1987. Strong localization of photons in certain disordered dielectric superlattices. *Phys. Rev. Lett.* 58:2486–89

70. Sigmund O, Hougaard K. 2008. Geometric properties of optimal photonic crystals. *Phys. Rev. Lett.* 100:153904
71. Rechtsman MC, Jeong HC, Chaikin PM, Torquato S, Steinhardt PJ. 2008. Optimized structures for photonic quasicrystals. *Phys. Rev. Lett.* 101:073902
72. Florescu M, Torquato S, Steinhardt PJ. 2009. Complete band gaps in two-dimensional photonic quasicrystals. *Phys. Rev. B* 80:155112
73. Florescu M, Torquato S, Steinhardt PJ. 2009. Designer disordered materials with large complete photonic band gaps. *Proc. Natl. Acad. Sci. USA* 106:20658–63
74. Sigmund O, Sondergaard JJ. 2003. Systematic design of phononic band-gap materials and structures by topology optimization. *Philos. Trans. R. Soc. London Ser. A* 100:1001–19
75. Torquato S. 1999. Exact conditions on physically realizable correlation functions of random media. *J. Chem. Phys.* 111:8832–37
76. Torquato S. 2006. Necessary conditions on realizable two-point correlation functions of random media. *Ind. Eng. Chem. Res.* 45:6293–98
77. Quintanilla J. 2008. Necessary and sufficient conditions for the two-point probability function of two-phase random media. *Proc. R. Soc. London Ser. A* 464:1761–79
78. Joshi MY. 1974. *A Class of Stochastic Models for Porous Media*. PhD thesis, Univ. Kansas, Lawrence
79. Roberts AP, Teubner M. 1995. Transport properties of heterogeneous materials derived from Gaussian random fields: bounds and simulation. *Phys. Rev. E* 51:4141–54
80. Torquato S, Stell G. 1982. Microstructure of two-phase random media. I. The *n*-point probability functions. *J. Chem. Phys.* 77:2071–77
81. Torquato S, Stell G. 1983. Microstructure of two-phase random media. II. The Mayer–Montroll and Kirkwood–Salsburg hierarchies. *J. Chem. Phys.* 78:3262–72
82. Lu BL, Torquato S. 1990. *n*-point probability functions for a lattice model of heterogeneous media. *Phys. Rev. B* 42:4453–59
83. Lu BL, Torquato S. 1992. Lineal-path function for random heterogeneous materials. *Phys. Rev. A* 45:922–29
84. Torquato S, Lu B. 1993. Chord-length distribution function for two-phase random media. *Phys. Rev. E* 47:2950–53
85. Torquato S, Beasley JD, Chiew YC. 1988. Two-point cluster function for continuum percolation. *J. Chem. Phys.* 88:6540–47
86. Jiao Y, Stillinger FH, Torquato S. 2009. A superior descriptor of random textures and its predictive capacity. *Proc. Natl. Acad. Sci. USA* 42:17634–39
87. Rintoul MD, Torquato S. 1997. Reconstruction of the structure of dispersions. *J. Colloid Interface Sci.* 186:467–76
88. Yeong CLY, Torquato S. 1998. Reconstructing random media. *Phys. Rev. E* 57:495–506
89. Basanta D, Miodownik MA, Holm EA, Bentley PJ. 2005. Investigating the evolvability of biologically inspired CA. *Metall. Mater. Trans. A* 36:1643–52
90. Ansari MA, Stepanek F. 2006. Design of granule structure: computational methods and experimental realization. *AIChE J.* 52:3762–74
91. Wu K, Van Dijke MIJ, Couples GD, Jiang Z, Ma J, et al. 2006. 3d stochastic modelling of heterogeneous porous media—applications to reservoir rocks. *Trans. Porous Media* 65:443–67
92. Kumar H, Briant WA, Curtin WA. 2006. Using microstructure reconstruction to model mechanical behavior in complex microstructures. *Mech. Mater.* 38:818–32
93. Cule D, Torquato S. 1999. Generating random media from limited microstructural information via stochastic optimization. *J. Appl. Phys.* 86:3428–37
94. Jiao Y, Stillinger FH, Torquato S. 2008. Modeling heterogeneous materials via two-point correlation functions. II. Algorithmic details and applications. *Phys. Rev. E* 77:031135
95. Yeong CLY, Torquato S. 1998. Reconstructing random media. II. Three-dimensional media from two-dimensional cuts. *Phys. Rev. E* 58:224–33
96. Manwart C, Hilfer R. 1999. Reconstruction of random media using Monte Carlo methods. *Phys. Rev. E* 59:5596–99

97. Sheehan N, Torquato S. 2001. Generating microstructures with specified correlation functions. *J. Appl. Phys.* 89:53–60
98. Jiao Y, Stillinger FH, Torquato S. 2007. Modeling heterogeneous materials via two-point correlation functions: basic principles. *Phys. Rev. E* 76:031110
99. Garboczi EJ, Bentz DP. 1998. Multi-scale analytical/numerical theory of the diffusivity of concrete. *J. Adv. Cement-Based Mater.* 8:77–88
100. Debye P, Anderson HR, Brumberger H. 1957. Scattering by an inhomogeneous solid. II. The correlation function and its applications. *J. Appl. Phys.* 28:679–83
101. Manwart C, Torquato S, Hilfer R. 2000. Stochastic reconstruction of sandstones. *Phys. Rev. E* 62:893–99
102. Hansen JP, McDonald IR. 1986. *Theory of Simple Liquids*. New York: Academic
103. Torquato S, Stillinger FH. 2002. Controlling the short-range order and packing densities of many-particle systems. *J. Phys. Chem. B* 106:8354–59. Erratum. 2002. *J. Phys. Chem. B* 106:11406
104. Torquato S, Stillinger FH. 2003. Local density fluctuations, hyperuniform systems, and order metrics. *Phys. Rev. E* 68:041113
105. Yamada M. 1961. Geometrical study of the pair distribution function in the many-body problem. *Prog. Theor. Phys.* 25:579–94
106. Costin O, Lebowitz J. 2004. On the construction of particle distributions with specified single and pair densities. *J. Phys. Chem. B.* 108:19614–18
107. Kuna T, Lebowitz JL, Speer ER. 2007. Realizability of point processes. *J. Stat. Phys.* 129:417–39
108. Torquato S, Stillinger FH. 2006. New conjectural lower bounds on the optimal density of sphere packings. *Exp. Math.* 15:307–31
109. Torquato S, Uche OU, Stillinger FH. 2006. Random sequential addition of hard spheres in high Euclidean dimensions. *Phys. Rev. E* 74:061308
110. Scardicchio A, Stillinger FH, Torquato S. 2008. Estimates of the optimal density of sphere packings in high dimensions. *J. Math. Phys.* 49:043301
111. Hopkins AB, Stillinger FH, Torquato S. 2009. Dense sphere packings from optimized correlation functions. *Phys. Rev. E* 79:031123
112. Crawford JR, Torquato S, Stillinger FH. 2003. Aspects of correlation function realizability. *J. Chem. Phys.* 119:7065–74
113. Uche OU, Stillinger FH, Torquato S. 2006. On the realizability of pair correlation functions. *Physica A* 360:21–36
114. Stillinger FH, Torquato S, Eroles JM, Truskett TM. 2001. Iso-$g^{(2)}$ processes in equilibrium statistical mechanics. *J. Phys. Chem. B* 105:6592–97
115. Sakai H, Stillinger FH, Torquato S. 2002. Equi-$g(r)$ sequences of systems derived from the square-well potential. *J. Chem. Phys.* 117:297–307
116. Stillinger FH, Torquato S. 2005. Realizability issues for iso-$g^{(2)}$ processes. *Mol. Phys.* 103:2943–49
117. Torquato S, Stillinger FH. 2006. Exactly solvable disordered sphere-packing model in arbitrary-dimensional Euclidean spaces. *Phys. Rev. E* 73:031106
118. Torquato S. 1986. Microstructure characterization and bulk properties of disordered two-phase media. *J. Stat. Phys.* 45:843–73
119. Torquato S. 2009. Inverse optimization techniques for targeted self-assembly. *Soft Matter* 5:1157–73